JACS
JOURNAL OF THE AMERICAN CHEMICAL SOCIETY
pubs.acs.org/JACS
Article

Exploring the Role of the Central Carbide of the Nitrogenase Active-Site FeMo-cofactor through Targeted ^{13}C Labeling and ENDOR Spectroscopy

Ana Pérez-González,[#] Zhi-Yong Yang,[#] Dmitriy A. Lukoyanov,[#] Dennis R. Dean,[*] Lance C. Seefeldt,[*] and Brian M. Hoffman[*]

Cite This: *J. Am. Chem. Soc.* 2021, 143, 9183–9190

ABSTRACT: Mo-dependent nitrogenase is a major contributor to global biological N_2 reduction, which sustains life on Earth. Its multi-metallic active-site FeMo-cofactor (Fe_7MoS_9C-homocitrate) contains a carbide (C^{4-}) centered within a trigonal prismatic CFe_6 core resembling the structural motif of the iron carbide, cementite. The role of the carbide in FeMo-cofactor binding and activation of substrates and inhibitors is unknown. To explore this role, the carbide has been in effect selectively enriched with ^{13}C, which enables its detailed examination by ENDOR/ESEEM spectroscopies. ^{13}C-carbide ENDOR of the $S = 3/2$ resting state (E_0) is remarkable, with an extremely small isotropic hyperfine coupling constant, $^{C}a = +0.86$ MHz. Turnover under high CO partial pressure generates the $S = 1/2$ hi-CO state, with two CO molecules bound to FeMo-cofactor. This conversion surprisingly leaves the small *magnitude* of the ^{13}C carbide isotropic hyperfine-coupling constant essentially unchanged, $^{C}a = -1.30$ MHz. This indicates that both the E_0 and hi-CO states exhibit an exchange-coupling scheme with nearly cancelling contributions to ^{C}a from three spin-up and three spin-down carbide-bound Fe ions. In contrast, the anisotropic hyperfine coupling constant undergoes a symmetry change upon conversion of E_0 to hi-CO that may be associated with bonding and coordination changes at Fe ions. In combination with the negligible difference between CFe_6 core structures of E_0 and hi-CO, these results suggest that in CO-inhibited hi-CO the dominant role of the FeMo-cofactor carbide is to maintain the core structure, rather than to facilitate inhibitor binding through changes in Fe-carbide covalency or stretching/breaking of carbide–Fe bonds.

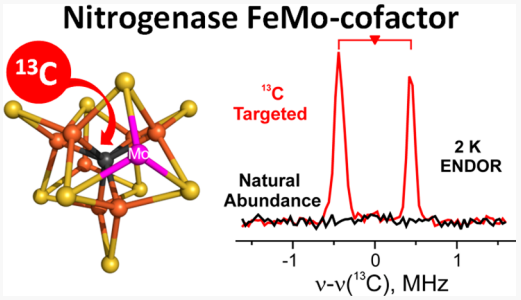

INTRODUCTION

The life-sustaining process of biological nitrogen fixation, the reduction of dinitrogen (N_2) to two ammonia (NH_3) molecules, is catalyzed by a suite of structurally and mechanistically similar isozymes, the nitrogenases.[1−9] The present work is focused on the Mo-dependent enzyme, the one most commonly found in nature and most thoroughly studied. For recent reviews see refs 10−12. Mo-dependent nitrogenase is composed of two catalytic partners designated the Fe protein and MoFe protein.[1] The Fe protein is an agent of nucleotide-dependent electron delivery to the MoFe protein, which contains the site of substrate binding and reduction. Substrate and inhibitor binding occurs at a complex organo-metallo-cofactor (Fe_7MoS_9C-homocitrate) called FeMo-cofactor. Figure 1A shows its structure in the MoFe protein resting state,[10] which by convention is designated E_0, as it has not acquired any reducing equivalents.[1] Reaction with substrates, or inhibitors such as CO, is achieved only under turnover conditions as FeMo-cofactor accumulates electrons and protons. The CO-inhibited state designated hi-CO is produced under turnover in the presence of a high concentration of CO.[1,13] ENDOR[14] and IR[15] spectroscopies have shown that FeMo-cofactor in the hi-CO state contains two coordinated CO molecules, one bound "end-on" to an Fe ion and a second that bridges two Fe ions, as beautifully visualized recently in an X-ray crystallographic structure,[16] Figure 1A.

A remarkable feature of FeMo-cofactor is the presence of a centrally located carbide (C^{4-}) within a Fe_6C trigonal prismatic core (Figure 1B). The identity of the central carbide within FeMo-cofactor was established by a high-resolution (1.0 Å) X-ray structure[17] and X-ray spectroscopy[18] of the MoFe protein (Figure 1A), while biosynthetic studies showed that it is derived from a methyl group provided by *S*-adenosyl-methionine (SAM)[19] (Figure 1C). Although the identity of the central carbide within the trigonally prismatic FeMo-cofactor CFe_6 core (Figure 1B) is firmly established, there is no information about what role it might play in FeMo-cofactor binding and activation of substrates and inhibitors. At one

Received: April 20, 2021
Published: June 10, 2021

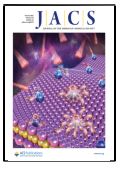

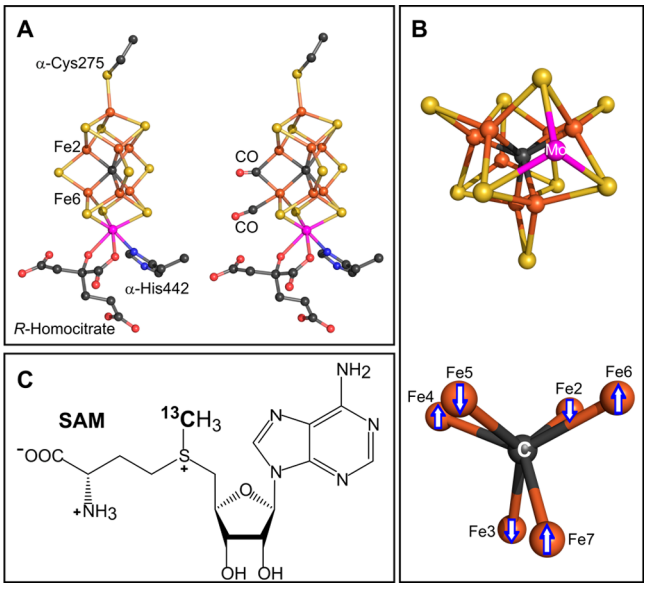

Figure 1. (A) Structure of FeMo-cofactor in the MoFe protein E_0 resting state (PDB: 3U7Q, left) and hi-CO state (PDB: 7JRF, right). Colors: Fe atoms in rust, Mo in magenta, S in yellow, C in dark gray, N in blue, and O in red. The two protein ligands, α-Cys^{275} and α-His^{442}, and *R*-homocitrate are shown. (B) FeMo-cofactor [Fe_7MoS_9C] unit looking down the Mo end (PDB: 3U7Q) (top) and the [Fe_6C] trigonal prismatic core (bottom). Arrows indicate orientations of Fe ion spins in the BS7 broken-symmetry exchange-coupling scheme (see text). (C) Structure of *S*-adenosyl-L-methionine (SAM) with a ^{13}C methyl group.

extreme, it may be that the CFe_6 core is simply a "heart of steel",[20] resembling the CFe_6 structural motif of cementite, the constituent of steels that gives them toughness.[21−24] In this view, the primary function of the Fe-carbide bonds is to hold the cofactor together as substrates and inhibitors bind to one or more of the Fe atoms through processes that may create open coordination sites by stretching or breaking one or more Fe−S bonds. At the other extreme, it may be that the Fe−C bonds provide a functionally dynamic (hemilabile) "beating heart", weakening or breaking to allow substrate or inhibitor binding to the associated Fe atom(s).[25−28] Labeling the carbide with ^{13}C would enable the use of ENDOR/ESEEM to monitor its properties, revealing where it resides on this spectrum of possible functions. Beyond that, as the carbide is literally "central" to FeMo-cofactor, measurements of the ^{13}C carbide hyperfine interactions with the electron spins of its surrounding Fe ions by ENDOR spectroscopy can serve as a reporter of *(i)* Fe-carbide bonding, *(ii)* the properties of the coordinated Fe ions themselves, *(iii)* exchange coupling among the metal ions, and *(iv)* how all these parameters change in turnover states that have bound substrates or inhibitors.

The present work shows that the approach to characterizing the central carbide with ^{13}C by using ^{13}C-glucose to generate a uniformly labeled MoFe protein,[29] even when carried out with complete isotopic incorporation,[17] does not provide a means to monitor and characterize the ^{13}C carbide of FeMo-cofactor. The problem: it is not possible to distinguish ENDOR/ESEEM signals associated with the central ^{13}C carbide from those of nearby ^{13}C-labeled amino acid residues in uniformly labeled ^{13}C enzyme. In any case, it would be prohibitively expensive to prepare sufficient amounts of uniformly enriched ^{13}C enzyme necessary to produce catalytic intermediates or inhibitor-bound states. Instead, a targeted genetic approach was developed that in effect selectively and quantitatively incorporates a ^{13}C carbide into FeMo-cofactor of functioning nitrogenase. ENDOR spectroscopy of the ^{13}C carbide in the enzyme thus enriched was then used to explore its properties in both the resting (E_0) state and the CO-inhibited state, hi-CO.

MATERIALS AND METHODS

Genetic Procedures, Cell Growth, Protein Purification, and MS Analysis of $^{13}C_5$-Methionine-Labeled MoFe Protein. The *Azotobacter vinelandii* strain DJ2396 used for ^{13}C labeling experiments is a derivative of DJ2102, which contains a Strep-tag-encoding sequence (ASWSHPQFEKN) placed at the N-terminus of NifD (MoFe protein α-subunit) for affinity purification purposes.[30,31] DJ2396 carries a streptomycin resistance-encoding insertion placed within the *metZ* gene that also results in the deletion of MetZ amino acid residues 74−393. DJ2396 requires the addition of L-methionine to sustain growth. Insertion of resistance cassettes within the *A. vinelandii* genome using transformation of competent cells has been previously described.[32] For large-scale culture, DJ2102 or DJ2396 cells were grown in a 150-L custom-built fermenter (W.B. Moore, Inc., Easton, PA) at 30 °C in modified Burk medium supplemented with 5.7 mM ammonium acetate as a fixed nitrogen source. Once the fixed nitrogen source was exhausted, cells were cultured for an additional 4 h and harvested. In the case of DJ2396, the culture medium was also supplemented with 50 μg/mL of L-methionine-(methyl-^{13}C) (Sigma-Aldrich). Affinity-tagged MoFe proteins and non-tagged Fe protein used in the present work were purified following previously described procedures.[30,31] Samples were analyzed by mass spectrometry using an Orbitrap Fusion Lumos mass spectrometer equipped with an Easy-nLC 1200 UPLC and an Easy Spray nanospray source, essentially as previously described.[33]

ESEEM and ENDOR Sample Preparation. Resting state samples of MoFe protein from DJ995[34] with no enrichment for ^{13}C incorporation and MoFe protein from DJ2396 with ^{13}C enrichment of the interstitial carbide in FeMo-cofactor by the protocol described above were each concentrated to about 300 μM in 50 mM Tris buffer at pH 8.0 with 250 mM NaCl and 2 mM dithionite, and about 420 μM in 50 mM Tris buffer at pH 8.0 with 500 mM NaCl and 2 mM dithionite, respectively. An aliquot of approximately 100 μL of each protein solution was transferred into a Q-band EPR tube, frozen in a hexane liquid/solid slurry, and then stored in liquid nitrogen. For X-band tubes, an aliquot of approximately 300 μL of each protein solution was transferred into the tube, frozen in a hexane slurry, and then stored in liquid nitrogen. hi-CO turnover samples were prepared by adding concentrated Fe protein to vials that contained 1 atm partial pressure of CO and a liquid phase composed of a MgATP regeneration system having final concentrations of 20 mM ATP, 20 mM $MgCl_2$, 24 mM phosphocreatine, 1.0 mg/mL BSA, 0.3 mg/mL creatine phosphokinase, and 40 mM sodium dithionite in a 200 mM MOPS buffer, pH 7.3. MoFe protein was added first to a final concentration of ~150 μM, and then the reaction was initiated by addition of Fe protein to a final concentration of ~120 μM. After 25 s of reaction at room temperature, 100 μL of the reaction solution was transferred to a Q-band EPR tube under 1 atm partial pressure of CO, frozen in a hexane slurry, and stored in liquid nitrogen.

ENDOR Spectroscopy. Q-band CW EPR spectra were collected at 2 K on a spectrometer with a helium immersion Dewar as previously reported.[35] Q-band pulsed Davies, Mims,[36] and ReMims[37] ENDOR spectra were collected at 2 K on a spectrometer with a helium immersion Dewar as previously reported.[38] The intensity of the ENDOR response for the Mims sequence, [$\pi/2$-τ-$\pi/2$-T(rf)-$\pi/2$-τ-detect],[36] follows the response function, $I(A) \sim 1 - \cos(2\pi A\tau)$,[36,27] and as a result, the signals at $A\tau = n$, $n = 0, 1, \ldots$, are suppressed ("blind spots").[36] The Doan/ReMims sequence, [$\pi/2$-τ_1-$\pi/2$-T(rf)-$\pi/2$-τ_2-π-(τ_1+τ_2)-detect], allows use of a short preparation interval τ_1 and study of a wider range of hyperfine values without "blind spot" distortions.[37] The simulations of 2D field-frequency plots of ENDOR

https://doi.org/10.1021/jacs.1c04152
J. Am. Chem. Soc. 2021, 143, 9183−9190

spectra collected across the EPR envelopes of E_0 and hi-CO, presented below, were carried out with lab-written programs as described.[39−41] Details of the analysis required to derive ^{13}C-carbide hyperfine tensors are presented in the Supporting Information (SI).

RESULTS AND DISCUSSION

^{13}C Labeling of the Central Carbide. A variety of experiments have demonstrated that the *S*-methyl of SAM (Figure 1C) is the carbide source for FeMo-cofactor,[42] which is ultimately derived from the terminal methyl (C_5) of the SAM precursor, methionine. This information indicated it might be possible to in effect selectively label the central carbide with ^{13}C by producing a nitrogen fixing organism, in this case *A. vinelandii*, that requires L-methionine to support growth. Therefore, a strain of *A. vinelandii* genetically disabled for the endogenous L-methionine biosynthetic pathway was isolated and optimized for growth under nitrogen-fixing conditions using exogenously supplied ^{13}C L-methionine. Mass spectrometry was used as a proxy for determination of ^{13}C labeling efficiency by analysis of a peptide fragment from the MoFe protein α-subunit that contains two methionine residues obtained from enzyme produced in cells supplemented with either $^{13}C_5$ or $^{12}C_5$ L-methionine, Figure 2. This

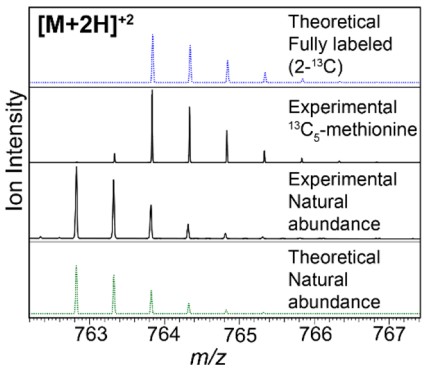

Figure 2. Incorporation of ^{13}C methionine into MoFe protein with high efficiency. The theoretical isotope distribution patterns for both the natural abundance and fully labeled (2-^{13}C) NifD (MoFe protein α-subunit) peptide (DMDMTLNNP*CWK) are shown below and above the experimentally determined patterns. The NifD peptide shown is doubly charged with a carbamidomethylated cysteine (*). Monoisotopic masses $[M+2H]^{+2}$: 762.8176 and 763.8210 for natural abundance and labeled, respectively. MS/MS analysis confirmed the methionine residues as the sites of ^{13}C incorporation.

analysis revealed greater than 99% incorporation of $^{13}C_5$ L-methionine into the peptide, with no scrambling of label to other amino acids, and hence, by inference, equivalent ^{13}C labeling of FeMo-cofactor. As now described, ENDOR measurements directly confirm the highly efficient ^{13}C labeling of FeMo-cofactor.

It should be emphasized that, although the targeted enrichment procedure also incorporates ^{13}C into the C_5-methyl position of all methionine residues and, therefore, is not strictly specific to the FeMo-cofactor carbide, in effect this is the outcome. There is no possibility for the protein matrix to contribute to ENDOR/ESEEM measurements reported here because the MoFe protein X-ray structures show there are no methionine residues in the vicinity of FeMo-cofactor. For example, in E_0 the shortest distance from a methionine-$^{13}CH_3$ to a FeMo-cofactor Fe is ∼9 Å (Figure S1).[17]

EPR Spectroscopy of Resting and hi-CO States. FeMo-cofactor within the MoFe protein E_0 state has a true electron spin, $S = 3/2$, but its EPR spectrum is commonly discussed in terms of a fictitious spin, $S' = 1/2$, and described by an *effective* g-tensor characterized by *g*-values, $\mathbf{g}' = [g_1', g_2', g_{||}] = [4.30, 3.67, 2.01]$,[1,43,44] with an orientation relative to FeMo-cofactor that has been determined by single-crystal EPR.[45] The hi-CO state has a true spin $S = 1/2$, and its EPR spectrum exhibits an axial g-tensor, $g_{||} = 2.17$, $g_{\perp} = 2.06$.[13] The actual spectra are displayed below, when presenting ENDOR spectra.

ENDOR Spectroscopy of ^{13}C-FeMo-cofactor in Resting and hi-CO States. Figure 3 presents the 35 GHz 2 K

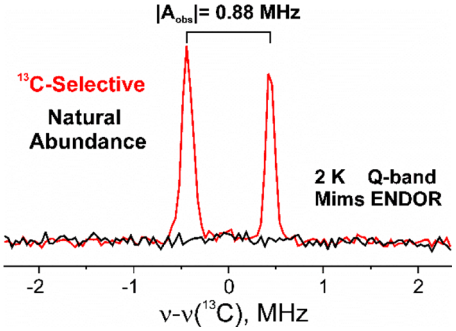

Figure 3. g = 2.035 35 GHz 2 K Mims ENDOR spectra of FeMo-cofactor with targeted ^{13}C labeling (red) and natural abundance (black). Conditions as in Figure 4, except for τ = 600 ns.

pulsed ^{13}C Mims ENDOR spectrum of ^{13}C-FeMo-cofactor at $g_{||} = 2.035$ of E_0, which interrogates only those enzymes in which the magnetic field lies along the $g_{||}$ axis ("single-crystal-like" position). The spectrum is remarkable, having an extraordinarily sharp doublet centered at the ^{13}C Larmor frequency with an extremely small observed hyperfine splitting $|A_{obs}| = 0.88$ MHz, which almost precisely corresponds to the magnitude of the ^{13}C isotropic coupling constant (see below). Because of the labeling procedure, this signal, which is reproduced with lower resolution in the corresponding X-band ESEEM spectrum (Figure S2), is unambiguously assigned to the ^{13}C-labeled central carbide.

Comparison of an X-band ESEEM spectrum of the E_0 state of MoFe protein that is in effect selectively ^{13}C-labeled, with the previously reported $g_{||}$ X-band ESEEM spectrum of uniformly ^{13}C-labeled MoFe protein prepared from cells grown using labeled ^{13}C glucose (Figure S2),[17] demonstrates the importance of targeted labeling. The previous ESEEM spectrum is notable for a strong signal from weakly-coupled ^{13}C that maximizes at the ^{13}C Larmor frequency and arises from the ^{13}C-labeled residues in the vicinity of FeMo-cofactor. The breadth of this "distant ESEEM" response effectively subsumes the actual ^{13}C-carbide signal from FeMo-cofactor which, based on the present results now can be recognized as contributing ill-resolved shoulders on the signal from the protein residues (Figure S2). In contrast, the absence of ^{13}C ENDOR (Figure 3) or ESEEM (Figure S2) responses at the ^{13}C Larmor frequency upon targeted labeling of the enzyme (also see below) confirms the remarkable selectivity of the labeling procedure, which alone enables high-precision ENDOR measurements of ^{13}C hyperfine coupling from the carbide. A ^{13}C signal seen previously in uniformly labeled enzyme, with observed $g_{||}$ hyperfine coupling, $|A_{obs}| = 2.5$ MHz[17] (Figure S2) is absent in the spectrum of enzyme with

https://doi.org/10.1021/jacs.1c04152
J. Am. Chem. Soc. 2021, 143, 9183−9190

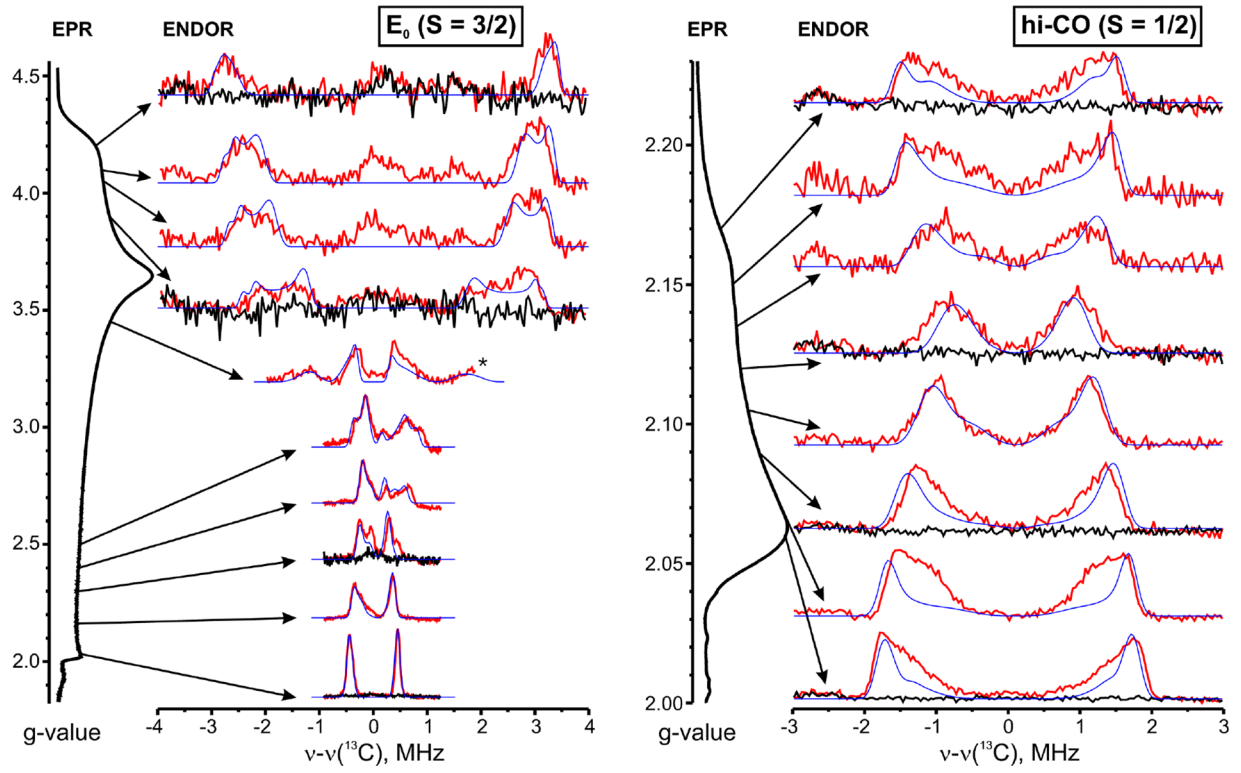

Figure 4. 2D field/frequency patterns of 35 GHz pulsed ENDOR spectra of FeMo-cofactor in resting and hi-CO states: (red) with targeted ^{13}C labeling, (black) natural abundance, and (blue) simulations. ENDOR spectra for E_0 and hi-CO are keyed to their corresponding absorption-display EPR envelopes as plotted on a *g*-value axis; each arrow connects an ENDOR spectrum with the *g*-value at which it was taken. Left, E_0: Treating the $S = 3/2$ state of E_0 as a fictitious spin, $S' = 1/2$, the simulation yields hyperfine tensor, $^{C}\boldsymbol{A}' = [+6.66, +0.79, -0.95]$ MHz; simulations actually input the $S = 3/2$ true spin tensor (see text), with rotation angles $\alpha = 0°$, $\beta = 2°$, $\gamma = 0°$, relative to the $\mathbf{g}'$ coordinate frame (in actuality the frame of the $S = 3/2$ zero-field splitting tensor). (*) Denotes interference from the third harmonic of ^{1}H ENDOR response. Right, hi-CO: Direct simulation of this 2D pattern for the $S = 1/2$ state yields $^{C}\boldsymbol{A} = [+3.2, -3.4, -3.7]$ MHz, with rotation angles $\alpha = 0°$, $\beta = 5°$, $\gamma = 15°$. The simulations and uncertainties in the resulting hyperfine tensor parameters are discussed in the SI. Conditions: EPR, microwave frequency 34.70 GHz (E_0) and 34.82 GHz (hi-CO), microwave power 10 μW, modulation amplitude 1 G, scan time 4 min; ENDOR, E_0, Mims (narrow scans) and Davies (wide scans), microwave frequency ~34.64 GHz, $t(\pi/2) = 50$ ns (Mims) and 40 ns (Davies), $\tau = 500$ ns (Mims) and 600 ns (Davies), $T_{RF} = 40$ μs, repetition time 10 ms; ENDOR, hi-CO, ReMims, microwave frequency ~34.72 GHz, $t(\pi/2) = 30$ ns, $\tau_1 = 140$ ns, $T_{RF} = 40$ μs, repetition time 50 ms.

targeted ^{13}C labeling (Figure 3). It was provisionally assigned to the carbide, but by ruling out that possibility the present results lead us to assign that signal to the β-^{13}C of α-subunit residue Cys[275] coordinated to the terminal Fe (Fe1) of FeMo-cofactor (Figure 1A).

To understand the interactions of the carbide ^{13}C with the cofactor electron spin in the $S = 3/2$ E_0 and $S = 1/2$ hi-CO states, the complete ^{13}C hyperfine tensors were determined for both states. Determining these tensors requires measurements of how the ENDOR spectra vary with the relative orientation of FeMo-cofactor and the external magnetic field. The full orientation dependence of a frozen solution is contained in a 2D field-frequency ("orientation-selective") pattern of ENDOR spectra taken at multiple fields across the EPR envelope,[39,40] as shown in Figure 4 for both E_0 and hi-CO. The complete ^{13}C carbide hyperfine tensor for E_0, as expressed relative to the fictitious spin $S' = 1/2$, denoted $^{C}\boldsymbol{A}'$, was determined from analysis[39,40,46] of the 2D pattern of Figure 4, left panel. The simulation of this pattern gives the relative signs of the resulting hyperfine tensor components; the absolute sign was determined from the so-called "pseudo-nuclear Zeeman" shift of the apparent ^{13}C Larmor frequency[47] (see SI). The three tensor elements, $^{C}\boldsymbol{A}' = [A_1', A_2', A_3']$ are listed in the legend to Figure 4. These elements are related to those for the ^{13}C carbide hyperfine tensor relative to the E_0 true spin 3/2, $^{C}\boldsymbol{A} = [A_1, A_2, A_3]$, by the relationship $^{C}\boldsymbol{A}' = [(g_1'/g_e)A_1, (g_2'/g_e)A_2, A_3]$.[36,37] Use of this expression yields $^{C}\boldsymbol{A} = [+3.10, +0.43, -0.95]$ MHz for the ^{13}C carbide of E_0. The hyperfine tensor $^{C}\boldsymbol{A}$ for hi-CO relative to its true spin $S = 1/2$ was directly determined by simulation of the 2D pattern of Figure 4, right panel, in conjunction with use of the PESTRE technique[48] to determine absolute signs (see SI). The tensor elements are $^{C}\boldsymbol{A} = [+3.2, -3.4, -3.7]$ MHz.[48]

Parenthetically, to emphasize the necessity of using targeted ^{13}C labeling to study the carbide, we note that only now, and only by comparison, can one realize that it was impossible to identify the ^{13}C carbide doublet in the previously reported $g' \approx 3.6$ ^{13}C ENDOR spectrum of (partially) uniformly enriched E_0 MoFe protein:[29] that doublet is completely subsumed in the very weak, unresolved trailing edges of the "distant ENDOR" signal from the many other ^{13}C in the uniformly enriched spectrum (Figure S3). This, perhaps surprisingly, shows that even the complete uniform ^{13}C incorporation[17] cannot enable determination of the ^{13}C-carbide hyperfine tensor.

The tensor elements for the true spin hyperfine coupling tensor $^{C}\boldsymbol{A}$ for each state are the sum of an isotropic coupling constant, ^{C}a, and the elements of an anisotropic interaction tensor, $^{C}\boldsymbol{T} = [T_1, T_2, T_3]$: $^{C}\boldsymbol{A} = [^{C}a + T_1, ^{C}a + T_2, ^{C}a + T_3]$.

https://doi.org/10.1021/jacs.1c04152
J. Am. Chem. Soc. 2021, 143, 9183−9190

This decomposition of the E_0 hyperfine tensor $^{C}\boldsymbol{A}$ yields an extremely small isotropic coupling constant, ^{C}a = +0.86 MHz, associated with a correspondingly small *net* spin density in the carbide 2s orbital. It further yields an unusual, small and near-rhombic anisotropic coupling tensor, $^{C}\boldsymbol{T}$ = [+2.24, −0.43, −1.81] MHz, where a fully rhombic tensor would have the form $^{C}\boldsymbol{T}$ = [+T, 0, −T]. Decomposition of the ^{13}C carbide hyperfine tensor of hi-CO, $^{C}\boldsymbol{A}$, shows that conversion of E_0 to hi-CO gives an isotropic coupling constant for the ^{13}C carbide of comparably small magnitude, ^{C}a = −1.30 MHz. In the following, we explain why the similar magnitudes of ^{C}a are significant but the different signs are not. Unlike ^{C}a, the conversion to hi-CO sharply changes the anisotropic coupling tensor, converting it to approximately axial ("dipolar") symmetry: $^{C}\boldsymbol{T}$ = [+4.5, −2.1, −2.4] MHz ≈ [2T, −T, −T]. We discuss this below, as well.

Origin of the ^{13}C-Carbide Hyperfine Coupling. Given that the ^{13}C carbide is covalently bonded to six high-spin Fe ions (Figure 1), it might have been imagined that spin delocalization in each Fe−C bond of E_0 would sum to a large ^{13}C-carbide 2s orbital spin density with correspondingly large isotropic hyperfine coupling constant, contrary to the observation here. For comparison, the 2.5 MHz coupling[17] assigned above to the ^{13}C β-carbon of α-subunit Cys^{275}, which is bound to the terminal Fe ion through an intervening sulfur, is nonetheless nearly 3-fold larger.[17] As a result, the observation of a small ^{13}C-carbide coupling might instead be interpreted as an indication that the anionic carbide merely ionically stabilizes the FeMo-cofactor without appreciable covalent spin delocalization from the iron ions to which it is bound. The comparable magnitude of the isotropic coupling constant for hi-CO upon binding two CO with loss of a sulfur would then be interpreted similarly.

However, such ideas do not take into account that the magnitudes of the contributions from the six "belt" Fe ions are not simply additive: the contributions from the different Fe ions carry differing signs as imposed by weighting factors (vector-coupling coefficients)[29] associated with the scheme that describes the exchange-coupling among the metal ions of the FeMo-cofactor. As a result, the small observed magnitudes of the isotropic coupling in the two states are not a direct measure of the spin delocalization through an individual Fe−C bond, as it would be for a mononuclear Fe ion.

Considering first E_0, Density Function Theory (DFT) computations and ^{57}Fe ENDOR measurements[29,49−52] suggest that exchange-coupling among the full complement of FeMo-cofactor metal ions in E_0 would favor a ground state with the so-called "BS7" exchange-coupling scheme, in which three of the six "belt" Fe ions bonded to the carbide are "spin-up (↑)" and three are "spin-down (↓)", schematically denoted (3↑/3↓). These spins are arranged in antiferromagnetically coupled (↑/↓) pairs at the edges of the trigonal prism of Fe ions, as illustrated in Figure 1B. As the hyperfine-coupling contributions of (↑) and (↓) Fe ions have opposite signs, in this scheme the opposing contributions from the spin-up and spin-down Fe ions strongly cancel, and it is this cancellation that results in the small magnitude of the observed ^{C}a.[29,52] Interestingly, the DFT computations find a second exchange-coupling scheme, denoted "BS6", slightly higher in energy but within the DFT uncertainty. However, BS6 has four up spins and two down in the trigonal prism (4↑/2↓). This would not exhibit such cancellation, and hence would lead to ^{C}a of far greater magnitude.[29,52] Thus, the ENDOR of the ^{13}C carbide of E_0 clearly identifies its ground state as the BS7 configuration.

There are two distinct ways in which formation of the inhibitor-bound hi-CO state *might have* substantially changed the ^{13}C-carbide hyperfine coupling constant. Firstly, of course, changes in the Fe-carbide bonds of the Fe ions that bind CO can modify the individual contributions of the Fe ions to the carbide isotropic coupling. In the limit where substrate binding is enabled by breaking one or more C−Fe bonds to create open coordination sites on those Fe ions, contributions to the ^{13}C-carbide ^{C}a from those Fe sites would be eliminated. At least in some cases this could paradoxically increase the coupling by lifting the cancellation of (↑/↓) Fe spin contributions in E_0. Secondly, like many species trapped under turnover conditions, hi-CO has an S = 1/2 FeMo-cofactor state. If the FeMo-cofactor E_0 S = 3/2 cluster with its (3↑/3↓) configuration were converted to an S = 1/2 cluster with a (4↑/2↓) exchange-coupling scheme, as noted above this would lift the cancellation condition on ^{C}a. In short, changes in structure that involve lengthening/breaking of an Fe−C bond(s), or a change in exchange-coupling configuration, or a combination of both *could* cause a dramatic increase in the magnitude of ^{C}a for hi-CO.[29,52] As next discussed, when one combines the absence of such an increase with the recently revealed crystallographic structure of hi-CO,[16] together they indicate that hi-CO, like E_0, exhibits a (3↑/3↓) configuration, presumably BS7.

The crystal structure of MoFe protein in the hi-CO state[16] shows that the binding of two CO to FeMo-cofactor causes minimal changes in the Fe−C bond lengths relative to the 1.0 Å E_0 structure,[17] despite the binding of two CO and loss of the sulfide ion that bridges Fe2 and Fe6. Thus, in E_0, the average of the six trigonal prismatic Fe−C distances is 2.00 (0.01) Å, with the C−Fe6 distance of 2.07 Å the longest. In hi-CO, the average distance is the same, within error (1.99 (0.02) Å), as is the C−Fe6 distance of 2.06 Å, even though Fe6 of hi-CO has adopted a five-coordinate trigonal bipyramidal geometry with bonds to both CO molecules, as opposed to the four-coordinate geometries of the other Fe ions in hi-CO and all Fe ions of E_0. Given this similarity in the core structures, it seems highly unlikely that the minimal increase in $|^{C}a|$ in hi-CO should be the result of large, but offsetting, *(i)* changes in individual Fe−C contributions to ^{C}a and *(ii)* changes in the summation over these contributions introduced by an altered exchange-coupling scheme as FeMo-cofactor goes from S = 3/2 to S = 1/2. We instead adopt the simplest interpretation—that the exchange-coupling schemes in E_0 and hi-CO exhibit equivalent (3↑/3↓) BS7 configurations.

This assignment further explains the finding that ^{C}a for the two states have similar small magnitudes, yet opposite signs. The above discussion shows that because the carbide interacts with six Fe ions, the sign of ^{C}a does not have the significance for analysis of bond covalency as it has in a simple metal−ligand system. With the FeMo-cofactor CFe_6 cores of hi-CO and E_0 both having three (↑) and three (↓) Fe ions, and with (↑/↓) ions giving hyperfine-coupling contributions of opposite sign, a small observed departure from ^{C}a = 0 MHz merely represents a small departure from exact cancellation of the opposing contributions. The opposite signs of ^{C}a simply reflect a slight excess contribution from (↓) Fe ions for E_0 and a comparably small excess contribution from the (↑) Fe ions for hi-CO.

https://doi.org/10.1021/jacs.1c04152
J. Am. Chem. Soc. 2021, 143, 9183−9190

In one sense, this proposed invariance in exchange-coupling scheme is perhaps not as surprising as the difference in FeMo-cofactor spin state and structures (Figure 1) would suggest. The hi-CO state only forms under turnover and is EPR-active, consistent with its proposed formation through acquisition of two electrons.[6] However, the bridging CO is formally reduced by those two electrons (formaldehyde level), while the terminal CO is merely a weak dative ligand. Thus, the FeMo-cofactor metal ion core of hi-CO remains at the same formal valence state as E_0, just as it retains the (3↑/3↓) BS7-type exchange-coupling scheme. Extension of these studies to catalytic intermediates through the ^{13}C labeling procedure described here will provide tests of DFT predictions that some intermediates associated with reduction of N_2 and other substrates will exhibit order-of-magnitude increases in ^{C}a.[29,52]

The anisotropic hyperfine coupling tensor, $^{C}\boldsymbol{T}$, of ^{13}C carbide behaves quite differently from the isotropic coupling. The contribution from an individual bonded Fe ion is well approximated by a sum of contributions from spin density in a carbon 2s-2p hybrid orbital directed toward the Fe and the through-space direct interaction of the Fe spin with the ^{13}C. Both of these, and therefore their sum, are of essentially dipolar symmetry with the symmetry axis along the particular Fe−C bond direction. Because the dipolar interaction tensors of the six Fe ions are non-coaxial, their sum in general does not cancel even when the sum of the isotropic couplings does. Considering $^{C}\boldsymbol{T}$ of E_0, its rhombic symmetry is a signature of dipolar interactions with a pair of Fe ions.[50] The BS7 exchange-coupling scheme of Figure 1B exhibits three antiferromagnetically ordered (spin-up, ↑/spin-down, ↓) pairs of spins along the edges of the Fe_6 trigonal prism. However, the pairs do not all have the same "phase": one of the pairs is (↓/↑), while the other two are (↑/↓). There are three possible positions of that out-of-phase pair ("rotamers"), and the unsymmetrical active-site environment causes them to have slightly different energies. Careful consideration of both the orientation of $^{C}\boldsymbol{T}$ relative to the FeMo-cofactor molecular frame and the magnitude of its components will distinguish which among these rotamer states is the ground state. In contrast, the axial symmetry of $^{C}\boldsymbol{T}$ in hi-CO is suggestive that it is dominated by change to a single Fe ion; if so, Fe6, with its distinctly different coordination geometry compared to other Fe sites in either state, is the obvious candidate.

Looking forward to future studies of intermediates trapped during substrate reduction, the present results clearly show that the ^{13}C carbide hyperfine tensor will provide a powerful guide for quantum mechanical computations aimed at reproducing the properties of FeMo-cofactor in its various catalytic states. In particular, the combined consideration of isotropic and anisotropic hyperfine coupling interactions will provide signatures of the operative FeMo-cofactor exchange-coupling scheme.

SUMMARY

The development of a means to prepare MoFe protein with targeted ^{13}C labeling of the central FeMo-cofactor carbide has made it possible to use ENDOR spectroscopy to sensitively and precisely monitor the electronic properties of the carbide and the spin-coupling scheme adopted by the FeMo-cofactor metal ions, both in the resting state and in states generated under turnover conditions. In the resting state, it is proposed the observed net isotropic coupling constant observed, ^{C}a = +0.86 MHz is near-zero because the sum of the isotropic hyperfine contributions from three "spin-up Fe" ions in the 6Fe belt of the C-Fe_6 FeMo-cofactor core effectively cancels the sum for the three belt "spin-down Fe" ions (BS7 exchange-coupling scheme; Figure 1B).

Surprisingly, the magnitude of the isotropic coupling does not change significantly in the hi-CO species. This indicates that hi-CO, like E_0, also exhibits a (3↑/3↓) configuration of electron spins on the six Fe ions of the trigonal prism, and thus presumably the same exchange-coupling scheme (BS7) as E_0, despite the change in spin state ($S = 3/2 \rightarrow 1/2$) as well as the changes in coordination at Fe6 and to a lesser extent at Fe2. This, in turn, suggests that ^{13}C ENDOR measurement of ^{C}a for labeled carbide will likewise serve as a basis for evaluating spin-exchange models in trapped catalytic intermediates, a long-standing and unmet challenge. For example, earlier DFT computations suggested that major changes are to be expected in the properties of the carbide in certain trapped catalytic intermediates.[53]

In contrast, the ^{13}C carbide anisotropic hyperfine interaction tensor, $^{C}\boldsymbol{T}$, undergoes a qualitative change in symmetry upon formation of hi-CO. It is suggested that $^{C}\boldsymbol{T}$ provides insights both into details of the BS7 exchange-coupling scheme and into how the electronic properties of FeMo-cofactor are influenced by details of the structural and electronic-structure changes at the Fe ions in states trapped under turnover conditions.

In combination with the negligible difference in the structures of the CFe_6 cores of E_0 and hi-CO, these results suggest that, at least in this CO-inhibited state, the dominant role of the FeMo-cofactor carbide is to maintain the core structure, rather than to facilitate inhibitor binding through changes in Fe−C covalency or stretching/breaking of C−Fe bonds. Whether this is also the case for states trapped during catalysis, for example the E_4 state primed for N_2 binding by the accumulation of four electrons and protons, remains to be explored. Indeed, the results presented here demonstrate the promise of using ^{13}C carbide hyperfine interactions as a means to reveal how the carbide and Fe core of the FeMo-cofactor function in catalytic states of nitrogenase, and in doing so provide a guide to the development of computational models for these states.[49,50]

ASSOCIATED CONTENT

Supporting Information

The Supporting Information is available free of charge at https://pubs.acs.org/doi/10.1021/jacs.1c04152.

Location of closest methionine to FeMo-cofactor; comparison of ^{13}C ESEEM and ENDOR spectra of uniformly labeled nitrogenase and enzyme with targeted ^{13}C labeling; and details of analysis of 2D field-frequency patterns of nitrogenase carbide ^{13}C ENDOR spectra, including Figures S1−S7 (PDF)

Accession Codes

Nitrogenase molybdenum−iron protein alpha chain, NifD, UniProtKB P07328; nitrogenase molybdenum−iron protein beta chain, NifK, UniProtKB P07329; nitrogenase iron protein 1, NifH, UniProtKB P00459.

AUTHOR INFORMATION

Corresponding Authors

Brian M. Hoffman − *Department of Chemistry, Northwestern University, Evanston, Illinois 60208, United States;*

https://doi.org/10.1021/jacs.1c04152
J. Am. Chem. Soc. 2021, 143, 9183−9190

orcid.org/0000-0002-3100-0746; Email: bmh@northwestern.edu

Dennis R. Dean − *Department of Biochemistry, Virginia Tech, Blacksburg, Virginia 24061, United States;* orcid.org/0000-0001-8960-6196; Email: deandr@vt.edu

Lance C. Seefeldt − *Department of Chemistry and Biochemistry, Utah State University, Logan, Utah 84322, United States;* orcid.org/0000-0002-6457-9504; Email: lance.seefeldt@usu.edu

Authors

Ana Pérez-González − *Department of Biochemistry, Virginia Tech, Blacksburg, Virginia 24061, United States*

Zhi-Yong Yang − *Department of Chemistry and Biochemistry, Utah State University, Logan, Utah 84322, United States;* orcid.org/0000-0001-8186-9450

Dmitriy A. Lukoyanov − *Department of Chemistry, Northwestern University, Evanston, Illinois 60208, United States;* orcid.org/0000-0002-4542-1648

Complete contact information is available at: https://pubs.acs.org/10.1021/jacs.1c04152

Author Contributions

#A.P.-G., Z.-Y.Y., and D.A.L. contributed equally.

Notes

The authors declare no competing financial interest.

■ ACKNOWLEDGMENTS

We thank Alvaro Salinero-Lanzarote for performing cell growth. We thank the VT-Mass Spectrometry Incubator team for performing and providing interpretation of the LC-MS analyses. The LC-MS resources used in the work are maintained with funding from the Fralin Life Sciences Institute and well as the USDA-NIFA Hatch Program (VA-160085). We thank Matthew D. Krzyaniak for the collection of ESEEM data. This was supported through the Center for Molecular Quantum Transduction, an EFRC funded by the U.S. Department of Energy (DOE), Office of Science, Basic Energy Sciences (DE-SC0021314). Grants from the U.S. Department of Energy, Office of Science, Basic Energy Sciences supported genetic studies, protein production, trapping of states for study, and ENDOR spectroscopy (DE-SC0010687, DE-SC0010834, and DE-SC0019342 to L.C.S., D.R.D., and B.M.H.). EPR/ENDOR/ESEEM spectroscopies were also supported by grants from the NSF and NIH (MCB-1908587 and GM111097 to B.M.H.).

■ REFERENCES

(1) Burgess, B. K.; Lowe, D. J. Mechanism of Molybdenum Nitrogenase. *Chem. Rev.* **1996**, *96* (7), 2983−3012.

(2) Hales, B. J. Alternative nitrogenase. *Adv. Inorg. Biochem.* **1990**, *8*, 165−198.

(3) Eady, R. R. Structure-function relationships of alternative nitrogenases. *Chem. Rev.* **1996**, *96* (7), 3013−3030.

(4) Eady, R. R. Current status of structure function relationships of vanadium nitrogenase. *Coord. Chem. Rev.* **2003**, *237* (1), 23−30.

(5) Schneider, K.; Muller, A. Iron-Only Nitrogenase: Exceptional Catalytic, Structural and Spectroscopic Features. In *Catalysts for Nitrogen Fixation: Nitrogenases, Relevant Chemical Models, and Commercial Processes*; Smith, B. E., Richards, R. L., Newton, W. E., Eds.; Springer: Dordrecht, 2004; pp 281−307.

(6) Seefeldt, L. C.; Yang, Z. Y.; Lukoyanov, D. A.; Harris, D. F.; Dean, D. R.; Raugei, S.; Hoffman, B. M. Reduction of Substrates by Nitrogenases. *Chem. Rev.* **2020**, *120* (12), 5082−5106.

(7) Yang, Z.-Y.; Jimenez-Vicente, E.; Kallas, H.; Lukoyanov, D. A.; Yang, H.; Martin del Campo, J. S.; Dean, D. R.; Hoffman, B. M.; Seefeldt, L. C. The Electronic Structure of FeV-cofactor in Vanadium-Dependent Nitrogenase. *Chem. Sci.* **2021**, *12*, 6913−6922.

(8) Harwood, C. S. Iron-Only and Vanadium Nitrogenases: Fail-Safe Enzymes or Something More? *Annu. Rev. Microbiol.* **2020**, *74* (1), 247−266.

(9) Van Stappen, C.; Decamps, L.; Cutsail, G. E.; Bjornsson, R.; Henthorn, J. T.; Birrell, J. A.; DeBeer, S. The Spectroscopy of Nitrogenases. *Chem. Rev.* **2020**, *120* (12), 5005−5081.

(10) Einsle, O.; Rees, D. C. Structural Enzymology of Nitrogenase Enzymes. *Chem. Rev.* **2020**, *120* (12), 4969−5004.

(11) Dos Santos, P. C.; Fang, Z.; Mason, S. W.; Setubal, J. C.; Dixon, R. Distribution of nitrogen fixation and nitrogenase-like sequences amongst microbial genomes. *BMC Genomics* **2012**, *13*, 162.

(12) Addo, M. A.; Dos Santos, P. C. Distribution of Nitrogen-Fixation Genes in Prokaryotes Containing Alternative Nitrogenases. *ChemBioChem* **2020**, *21* (12), 1749−1759.

(13) Davis, L. C.; Henzl, M. T.; Burris, R. H.; Orme-Johnson, W. H. Iron-Sulfur Clusters in the Molybdenum-Iron Protein Component of Nigrogenase. Electron Paramagnetic Resonance of the Carbon Monoxide Inhibited State. *Biochemistry* **1979**, *18*, 4860−4869.

(14) Lee, H.-I.; Cameron, L. M.; Hales, B. J.; Hoffman, B. M. CO Binding to the FeMo Cofactor of CO-Inhibited Nitrogenase: ^{13}CO and ^{1}H Q-Band ENDOR investigation. *J. Am. Chem. Soc.* **1997**, *119*, 10121−10126.

(15) George, S. J.; Ashby, G. A.; Wharton, C. W.; Thorneley, R. N. F. Time-Resolved Binding of Carbon Monoxide to Nitrogenase Monitored by Stopped-Flow Infrared Spectroscopy. *J. Am. Chem. Soc.* **1997**, *119* (27), 6450−6451.

(16) Buscagan, T. M.; Perez, K. A.; Maggiolo, A. O.; Rees, D. C.; Spatzal, T. Structural Characterization of Two CO Molecules Bound to the Nitrogenase Active Site. *Angew. Chem., Int. Ed.* **2021**, *60* (11), 5704−5707.

(17) Spatzal, T.; Aksoyoglu, M.; Zhang, L. M.; Andrade, S. L. A.; Schleicher, E.; Weber, S.; Rees, D. C.; Einsle, O. Evidence for Interstitial Carbon in Nitrogenase FeMo Cofactor. *Science* **2011**, *334* (6058), 940−940.

(18) Lancaster, K. M.; Roemelt, M.; Ettenhuber, P.; Hu, Y.; Ribbe, M. W.; Neese, F.; Bergmann, U.; DeBeer, S. X-ray Emission Spectroscopy Evidences a Central Carbon in the Nitrogenase Iron-Molybdenum Cofactor. *Science* **2011**, *334* (6058), 974−977.

(19) Jasniewski, A. J.; Lee, C. C.; Ribbe, M. W.; Hu, Y. Reactivity, Mechanism, and Assembly of the Alternative Nitrogenases. *Chem. Rev.* **2020**, *120* (12), 5107−5157.

(20) Prof. Oliver Einsle, private communication that correlates a possible role of the FeMo-cofactor core with the role of cementite, with its similar structural motif.

(21) Sluiter, M. First principles in modelling phase transformations in steels. In *Phase Transformations in Steels*; Pereloma, E., Edmonds, D., Eds.; Woodhead Publishing: Cambridge, UK, 2017; pp 365−404.

(22) Bhadeshia, H. K. D. H. Cementite. *Int. Mater. Rev.* **2020**, *65* (1), 1−27.

(23) We note that the name of the mineral, cementite, with its CFe_6 structural units, was coined to imply that the carbide "cements" the Fe ions together.

(24) Grunenberg, J. The Interstitial Carbon of the Nitrogenase FeMo Cofactor is Far Better Stabilized than Previously Assumed. *Angew. Chem., Int. Ed.* **2017**, *56* (25), 7288−7291.

(25) Peters, J. C.; Mehn, M. P. Bio-organometallic Approaches to Nitrogen Fixation Chemistry. *Activation of Small Molecules* **2006**, 81−119.

(26) Čorić, I.; Holland, P. L. Insight into the Iron-Molybdenum Cofactor of Nitrogenase from Synthetic Iron Complexes with Sulfur, Carbon, and Hydride Ligands. *J. Am. Chem. Soc.* **2016**, *138* (23), 7200−11.

(27) Holland, P. L. Low-coordinate iron complexes as synthetic models of nitrogenase. *Can. J. Chem.* **2005**, *83* (4), 296−301.

(28) Ding, S.; Ghosh, P.; Darensbourg, M. Y.; Hall, M. B. Interplay of hemilability and redox activity in models of hydrogenase active sites. *Proc. Natl. Acad. Sci. U. S. A.* **2017**, *114* (46), E9775−E9782.
(29) Lukoyanov, D.; Pelmenschikov, V.; Maeser, N.; Laryukhin, M.; Yang, T. C.; Noodleman, L.; Dean, D.; Case, D.; Seefeldt, L.; Hoffman, B. Testing if the Interstitial Atom, X, of the Nitrogenase Molybdenum-Iron Cofactor is N or C: ENDOR, ESEEM, and DFT Studies of the S = 3/2 Resting State in Multiple Environments. *Inorg. Chem.* **2007**, *46* (26), 11437−11449.
(30) Jiménez-Vicente, E.; Martin Del Campo, J. S.; Yang, Z.-Y.; Cash, V. L.; Dean, D. R.; Seefeldt, L. C. Application of affinity purification methods for analysis of the nitrogenase system from Azotobacter vinelandii. In *Methods in Enzymology*; Armstrong, F., Ed.; Academic Press: Cambridge, MA2018; Vol. *613*, Chap. 9, pp 231−255.
(31) Burgess, B. K.; Jacobs, D. B.; Stiefel, E. I. Large-scale purification of high activity *Azotobacter vinelandii* nitrogenase. *Biochimica et biophysica acta* **1980**, *614*, 196−209.
(32) Dos Santos, P. C. Molecular biology and genetic engineering in nitrogen fixation. *Methods Mol. Biol.* **2011**, *766*, 81−92.
(33) Jimenez-Vicente, E.; Yang, Z. Y.; Ray, W. K.; Echavarri-Erasun, C.; Cash, V. L.; Rubio, L. M.; Seefeldt, L. C.; Dean, D. R. Sequential and differential interaction of assembly factors during nitrogenase MoFe protein maturation. *J. Biol. Chem.* **2018**, *293* (25), 9812−9823.
(34) Christiansen, J.; Goodwin, P. J.; Lanzilotta, W. N.; Seefeldt, L. C.; Dean, D. R. Catalytic and Biophysical Properties of a Nitrogenase Apo-MoFe Protein Produced by a *nifB*-Deletion Mutant of *Azotobacter vinelandii*. *Biochemistry* **1998**, *37* (36), 12611−12623.
(35) Werst, M. M.; Davoust, C. E.; Hoffman, B. M. Ligand spin densities in blue copper proteins by Q-band ^{1}H and ^{14}N ENDOR spectroscopy. *J. Am. Chem. Soc.* **1991**, *113* (5), 1533−1538.
(36) Schweiger, A.; Jeschke, G. *Principles of Pulse Electron Paramagnetic Resonance*; Oxford University Press: Oxford, UK, 2001; pp 1−578.
(37) Doan, P. E.; Hoffman, B. M. Making hyperfine selection in Mims ENDOR independent of deadtime. *Chem. Phys. Lett.* **1997**, *269*, 208−214.
(38) Davoust, C. E.; Doan, P. E.; Hoffman, B. M. Q-band pulsed electron spin-echo spectrometer and its application to ENDOR and ESEEM. *J. Magn. Reson., Ser. A* **1996**, *119* (1), 38−44.
(39) Hoffman, B. M.; DeRose, V. J.; Doan, P. E.; Gurbiel, R. J.; Houseman, A. L. P.; Telser, J. Metalloenzyme Active-Site Structure and Function through Multifrequency CW and Pulsed ENDOR. *Biol. Magn. Reson.* **1993**, *13*, 151−218.
(40) DeRose, V. J.; Hoffman, B. M. Protein Structure and Mechanism Studied by Electron Nuclear Double Resonance Spectroscopy. In *Methods in Enzymology*; Sauer, K., Ed.; Academic Press: New York, 1995; Vol. *246*, pp 554−589.
(41) Doan, P. E.; Lees, N. S.; Shanmugam, M.; Hoffman, B. M. Simulating Suppression Effects in Pulsed ENDOR, and the 'Hole in the Middle' of Mims and Davies ENDOR Spectra. *Appl. Magn. Reson.* **2010**, *37* (1−4), 763−779.
(42) Hu, Y.; Ribbe, M. W. Nitrogenases—A Tale of Carbon Atom(s). *Angew. Chem., Int. Ed.* **2016**, *55* (29), 8216−8226.
(43) True, A. E.; Nelson, M. J.; Venters, R. A.; Orme-Johnson, W. H.; Hoffman, B. M. ^{57}Fe Hyperfine Coupling Tensors of the FeMo Cluster in *Azotobacter vinelandii* MoFe Protein: Determination by Polycrystalline ENDOR Spectroscopy. *J. Am. Chem. Soc.* **1988**, *110*, 1935−1943.
(44) Hoffman, B. M.; Gurbiel, R. J.; Werst, M. M.; Sivaraja, M. Electron Nuclear Double Resonance (ENDOR) of Metalloenzymes. In *Advanced EPR. Applications in Biology and Biochemistry*; Hoff, A. J., Ed.; Elsevier: Amsterdam, 1989; pp 541−591.
(45) Spatzal, T.; Einsle, O.; Andrade, S. L. A. Analysis of the Magnetic Properties of Nitrogenase FeMo Cofactor by Single-Crystal EPR Spectroscopy. *Angew. Chem., Int. Ed.* **2013**, *52* (38), 10116−10119.
(46) Doan, P. E. The Past, Present, and Future of Orientation-Selected ENDOR Analysis: Solving the Challenges of Dipolar-Coupled Nuclei. In *Paramagnetic Resonance of Metallobiomolecules*; Telser, J., Ed.; American Chemical Society: Washington, DC, 2003; pp 55−81.
(47) Abragam, A.; Bleaney, B. *Electron Paramagnetic Resonance of Transition Ions*, International Series of Monographs on Physics; Clarendon Press: Oxford, 1970; 925 pp.
(48) Doan, P. E. Combining steady-state and dynamic methods for determining absolute signs of hyperfine interactions: Pulsed ENDOR Saturation and Recovery (PESTRE). *J. Magn. Reson.* **2011**, *208* (1), 76−86.
(49) Raugei, S.; Seefeldt, L. C.; Hoffman, B. M. Critical computational analysis illuminates the reductive-elimination mechanism that activates nitrogenase for N_2 reduction. *Proc. Natl. Acad. Sci. U. S. A.* **2018**, *115* (45), No. E10521.
(50) Hoeke, V.; Tociu, L.; Case, D. A.; Seefeldt, L. C.; Raugei, S.; Hoffman, B. M. High-Resolution ENDOR Spectroscopy Combined with Quantum Chemical Calculations Reveals the Structure of Nitrogenase Janus Intermediate E4(4H). *J. Am. Chem. Soc.* **2019**, *141* (30), 11984−11996.
(51) Doan, P. E.; Telser, J.; Barney, B. M.; Igarashi, R. Y.; Dean, D. R.; Seefeldt, L. C.; Hoffman, B. M. ^{57}Fe ENDOR Spectroscopy and 'Electron Inventory' Analysis of the Nitrogenase E4 Intermediate Suggest the Metal-Ion Core of FeMo-cofactor Cycles Through Only One Redox Couple. *J. Am. Chem. Soc.* **2011**, *133* (43), 17329−17340.
(52) Pelmenschikov, V.; Case, D. A.; Noodleman, L. Ligand-Bound S = 1/2 FeMo-Cofactor of Nitrogenase: Hyperfine Interaction Analysis and Implication for the Central Ligand X Identity. *Inorg. Chem.* **2008**, *47*, 6162−6172.
(53) Lee, H.-I.; Sorlie, M.; Christiansen, J.; Song, R.; Dean, D. R.; Hales, B. J.; Hoffman, B. M. Characterization of an Intermediate in the Reduction of Acetylene by the Nitrogenase α-Gln^{195} MoFe Protein by Q-band EPR and ^{13}C,^{1}H ENDOR. *J. Am. Chem. Soc.* **2000**, *122* (23), 5582−5587.

https://doi.org/10.1021/jacs.1c04152
J. Am. Chem. Soc. 2021, 143, 9183−9190